Rotating states of self-propelling particles in two dimensions

Hsuan-Yi Chen[1,2,3] and Kwan-tai Leung[1,4]

[1]*Graduate Institute of Biophysics, National Central University, Jhongli, 32054 Taiwan, Republic of China*
[2]*Department of Physics, National Central University, Jhongli, 32054 Taiwan, Republic of China*
[3] *Center for Complex Systems, National Central University, Jhongli, 32054 Taiwan, Republic of China*
[4]*Institute of Physics, Academia Sinica, Taipei 11529, Taiwan, Republic of China*

We present particle-based simulations and a continuum theory for steady rotating flocks formed by self-propelling particles (SPPs) in two-dimensional space. Our models include realistic but simple rules for the self-propelling, drag, and interparticle interactions. Among other coherent structures, in particle-based simulations we find steady rotating flocks when the velocity of the particles lacks long-range alignment. Physical characteristics of the rotating flock are measured and discussed. We construct a phenomenological continuum model and seek steady-state solutions for a rotating flock. We show that the velocity and density profiles become simple in two limits. In the limit of weak alignment, we find that all particles move with the same speed and the density of particles vanishes near the center of the flock due to the divergence of centripetal force. In the limit of strong body force, the density of particles within the flock is uniform and the velocity of the particles close to the center of the flock becomes small.

I. INTRODUCTION

The collective motion of animal groups and bacteria colonies is one of the most fascinating nonequilibrium dynamical phenomena in the living world [1–3]. Under extreme conditions, bacteria colonies exhibit complex patterns due to the interplay between chemical signaling waves, nutrition diffusion, and motion of the bacteria [2,3]. Animal groups ranging from fish schools to bird flocks to ants also sometimes form interesting moving patterns [4]. An important question in statistical physics is to study the self-organizing principle in these biological systems. A recent review of the efforts over the past decade has been given by Toner *et al.* [5].

Among the complex patterns formed by animal and bacteria groups, the simple steady rotating flocks have received much attention from both theorists and experimentalists [1,4,6,7] but have not been well understood. The classic works of Toner, Tu, and collaborators have not discussed the rotating states of flocks in free space [8–10]. However, simulations for a two-dimensional (2D) particle-based model by Levine *et al.* [11] have shown this structure in a range of parameters. The existence of rotating states for relatively small flocks of 20 particles with Morse interaction was also demonstrated in [12], and it was pointed out that due to the influence of noise, the direction of rotation changes from time to time. Their study differs from [11] in that the rotational motion is induced by weak deviation from radial symmetry in the potential that acts on the particle. A similar model [13] is used to compare with the experimentally observed rotational motion in Daphnia under the action of an attractive light source [14]. Recently, in Ref. [1] Mikhailov and Calenbuhr studied the density and velocity profiles of the rotating states by a hydrodynamic continuum model which does not have the velocity-alignment interactions between the particles. In general, interesting questions regarding the condition under which steady rotating states of flocks can be observed, or the density and velocity distribution within

steady rotating states, are clearly of great experimental as well as theoretical interest [1].

In this paper we present particle-based simulations and a continuum theory for the dynamics of finite-size flocks formed by self-propelling particles (SPPs). In our models all particles are under self-propelling motion in a viscous environment which provides drag force on them. They are held together by some social interaction that tends to keep the nearest neighbors at a preferred distance. At the same time there is a tendency for them to move along the same direction as their neighbors. We study the solutions of these models in two dimensions, in particular we focus on the steady rotating states in both simulation and theory.

This paper is organized as follows. In Sec. II, we discuss the particle-based simulations. Various steady states observed are summarized, and the results for the rotating state are given. In Sec. III a continuum theory is constructed and steady rotating solutions in two dimensions are given. Section IV summarizes this paper.

II. A PARTICLE-BASED MODEL

A. Specification of the model

In a particle-based model, the motions of the particles obey Newtonian dynamics. The major distinction between a self-propelling particle and a passively driven one is that the former is powered to move by some internal mechanism that typically converts chemical energy into mechanical energy. As a result, on its own the particle reaches a stable motion at a constant speed. As in previous models of flocking [3,7,11,15], internal degrees of freedom such as those responsible for propelling, braking, and turning are all ignored, as they are irrelevant to the collective behavior being studied. Moreover, the particles are treated as identical for two reasons: first, different biological species normally do not
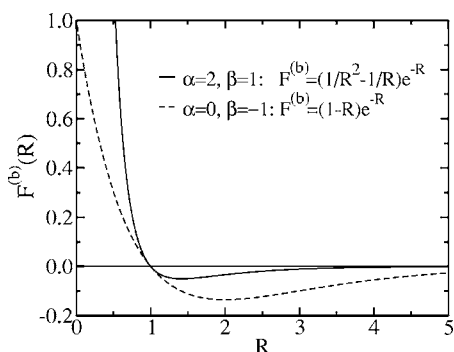
FIG. 1. The body force versus interparticle distance for particles with hard core ($\alpha=2$, $\beta=1$) and soft-core ($\alpha=0$, $\beta=-1$). $r_b=1$ here.

flock; second, it is our goal to study flocking without any particle being special (such as a leader).

Consider a system consisting of N identical particles then, each of mass m. For a particle at the position $\mathbf{r}_i$ with velocity $\mathbf{v}_i$, the equation of motion takes the following form:

$$m\frac{d\mathbf{v}_i}{dt} = -\gamma\mathbf{v}_i + \mathbf{F}_i^{(a)} + \mathbf{F}_i^{(b)} + \xi_i. \quad (1)$$

There are four types of force that act on the particle:

(*i*) The drag force $-\gamma\mathbf{v}_i$ that arises from the hydrodynamic or frictional nature of the medium.

(*ii*) The alignment force $\mathbf{F}_i^{(a)}$ that accounts for the self-propelling force and the tendency of the particle to align its velocity with its neighboring particles.

(*iii*) The body force $\mathbf{F}_i^{(b)}$ that accounts for the interaction with nearby particles.

(*iv*) A noise term ξ_i that both emphasizes the fact that the alignment is not perfect and models the effect of rapidly fluctuating environmental conditions.

In the context of biology, both the alignment and body force are not real, physical forces. They are derived from the social responses of an individual to other members of the same species. Consider the body force first. For flocking to happen, the particles need to attract each other to get close in the first place. Meanwhile, they would rather avoid colliding into each other. A simple form of the body force that satisfies these requirements is

$$\mathbf{F}_i^{(b)} = b\sum_{j\neq i}\hat{\mathbf{R}}_{ji}\left[\left(\frac{r_b}{R_{ji}}\right)^{\alpha} - \left(\frac{r_b}{R_{ji}}\right)^{\beta}\right]e^{-R_{ji}/r_b}. \quad (2)$$

In this equation, $\mathbf{R}_{ji}=\mathbf{r}_i-\mathbf{r}_j$, $\hat{\mathbf{R}}_{ji}$ is its unit vector, b is the force strength, and r_b is a screening length. The exponents $\alpha>\beta$ give rise to the desirable long-range attractive and short-range repulsive interaction. Many choices are possible, e.g., ($\alpha=2$, $\beta=1$) corresponds to the case of hard-core particles, whereas ($\alpha=0$, $\beta=-1$) corresponds to soft cores. Figure 1 shows the differences between these two cases. Compared to hard cores, soft cores make the particles gently repelling rather than bouncing off each other vigorously, leading to more densely packed flocks.

For the alignment force, we consider two variants:

$$\mathbf{F}_i^{(a)} = a\hat{\mathbf{V}}_i,$$

$$\mathbf{V}_i = \mathbf{v}_i + \sum_{j\neq i}\mathbf{v}_j e^{-R_{ji}/r_a}, \quad (3)$$

and

$$\mathbf{F}_i^{(a)} = a\mathbf{U}_i,$$

$$\mathbf{U}_i = \hat{\mathbf{v}}_i + \sum_{j\neq i}\hat{\mathbf{v}}_j e^{-R_{ji}/r_a}. \quad (4)$$

Similar to the body force, the alignment effect is screened beyond a finite range r_a. Unlike the body force, however, the factor $1/R^{\alpha}-1/R^{\beta}$ is absent because a switch from alignment to antialignment is not physical. For a particle traveling alone, $\mathbf{F}^{(a)}$ is nothing but a constant acceleration which due to damping eventually results in a constant speed a/γ. When surrounded by neighbors, the particle aligns itself along a direction determined by a weighted average over the velocities of those neighbors. The choices above are just two examples among many imaginable implementations of this alignment effect. They look similar with a subtle difference: The amplitude of the force in (4) increases as the number of neighboring particles increases, while it is constant in (3). They give rise to different flocking behavior. We shall mainly discuss the results for the first choice.

As usual, for a dynamical system a noise term is needed to equilibrate it toward a stable steady state. For simplicity, in simulations the noise has no spatial or temporal correlation. It is taken from a uniform distribution over $[-w,w]$.

Needless to say, our model is by no means unique. There is a great deal of freedom involved in its specification. Among previous works, the model of Ref. [7] has a similar body force but there is no alignment, whereas the model of Ref. [11] differs from ours in the functional form of the body force, and that they consider mainly the form displayed in Eq. (4) for the alignment. Generally speaking, since we do not model after a specific system (e.g., birds, fish, or bacteria), there is no *a priori* reason to favor one choice of the terms or parameters over another. In our view, the details of the model do not really matter as long as the resulting model makes sound physical and mathematical sense. Moreover, in building our model, we strive for a balance between realism and computational efficiency. With this model we address such basic questions as:

(1) Can flocking arise without a leader and a confining boundary?

(2) What are the possible phases of collective motion?

(3) What are the characteristics of those phases?

(4) What are the nature of the associated phase transitions?

As mentioned above, to address the first question all particles are treated as identical, and periodic boundary conditions (PBCs) are imposed to eliminate confinement. Analogous to a system of spins, a leader would correspond to a spin that has a stronger coupling to other spins than the rest, and the absence of a global force field is analogous to having zero external magnetic field.

The answer to the first question above is affirmative, as we shall see below. Answering the other questions requires a great deal of effort as the parameter space is huge and the phase diagram is complex and has a high dimension. For this reason, we shall only describe qualitatively the various phases observed, and focus our attention in this paper on one particular phase. The rich variety of phases of flocks predicted theoretically or observed experimentally are discussed in detail in [5].

B. The phases

In this paper, we only consider the model in two spatial dimensions. Initially the particles are distributed at random positions and velocities. The equations of motion are then solved numerically in continuous space and discrete time by the Euler method. The number of particles simulated ranges from tens to hundreds, and the system size is always sufficiently large ($L_x = L_y \equiv L \gg$ force ranges and flock size) to eliminate boundary effects. Of the many parameters, without loss of generality we choose the length and time scale such that the screening length r_b for the body force and the mass m are both unity. Unless otherwise stated, a soft-core body force in (2) with $\alpha = 0$ and $\beta = -1$, and a constant-amplitude alignment force as in (3) are employed. Of the remaining parameters, γ^{-1} is the relaxation time of the velocity and w determines the fluctuation of the system around steady states (e.g., how soon a flock changes its direction of motion). Neither are crucial to the qualitative characteristics of collective motion. Hence, they are also fixed($\gamma = 1$ and $w = 2$). The key parameters left are the screening length r_a for alignment, the strength a for acceleration and alignment, and the strength b for the body force.

If the body force is too weak to held the particles together, most of them would undergo independent free flight—the system is in a gas phase with at most some small clusters forming and dissociating dynamically. The only interesting scenario is when the body force is large enough for global structures to form. Therefore, hereafter we also fix $b = 1$ and consider the reduced phase space spanned by r_a and a. In other words, we concentrate on the effect of self-propulsion and alignment as they are believed to be the key factors responsible for flocking. From simulations, we find the following distinct steady states:

• Crystal: Under strong body forces without alignment and self-propelling, the system forms a stationary crystal. Given a fixed number of particles, the crystalline cluster has a definite close-packed structure that minimizes the interparticle energy, as shown in Fig. 2 (see [16] for an experimental realization). For finite a and a sufficiently large alignment range ($r_a \gtrsim 0.1$) greater than the interparticle distance, the velocities of the particles are strongly correlated to give rise to a marching crystal. A marching crystal phase is ubiquitous. Only at the corner of small r_a and a do we find other flocking structures.

• Swarm: At high noise level and finite a, positional order may be destroyed as the particles joggle vigorously. If r_a covers the extent of the cluster, there is velocity correlation but no positional order—the flock behaves like a swarm that
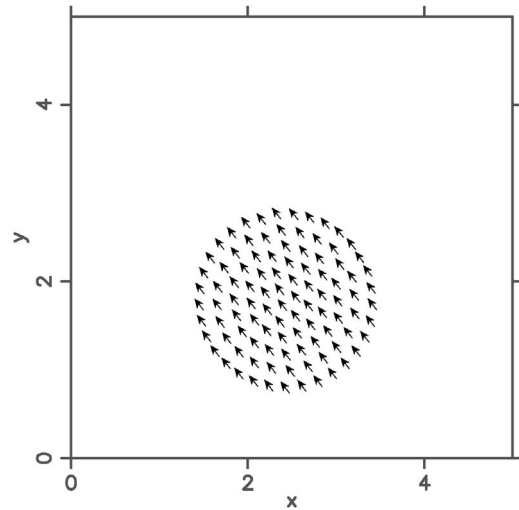

FIG. 2. A typical snapshot of a steady marching crystal, under strong alignment. Each particle is marked by an arrow proportional to its velocity. $N = 100$, $L = 10$, $a = 1$, $r_a = 1$, $b = 1$, $w = 2$.

drifts coherently together. See Fig. 3 for a typical snapshot. If r_a is too small, even velocity correlation is lost and the swarm cannot have any directed motion.

• Vortex: At small enough r_a, and $a \lesssim 1$, a fraction of random initial configurations may evolve into a stationary flock with particles rotating about a common center. Initially, some particles rotate clockwise while the rest rotate counterclockwise. In time, eventually they all rotate in the same sense (see Fig. 4). The alignment range r_a governs how fast this rotational alignment takes place. The rotating flock does not have directed motion. It is reminiscent of the vortices formed by certain species of fish, such as caranx sexfasciatus [17]. If r_a is increased gradually, the tendency to align competes with rotation. Eventually, at some critical value of r_a (that depends on several parameters, including a and N) the
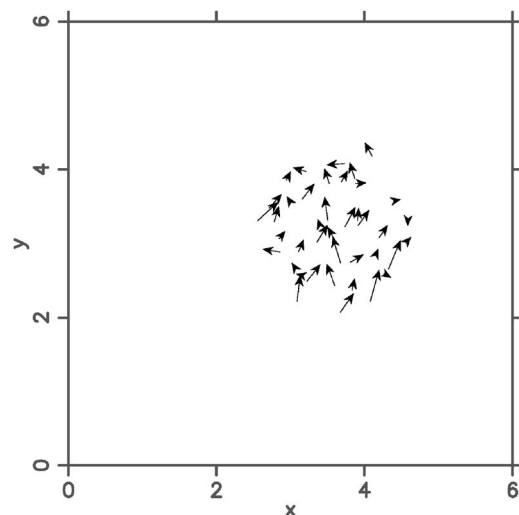

FIG. 3. A snapshot of the swarm state under strong noise. The flock drifts with a finite mean velocity, about which the particles weave randomly like a swarm of insects. $N = 40$, $L = 10$, $a = 0.2$, $r_a = 0.5$, $b = 1$, $w = 50$.
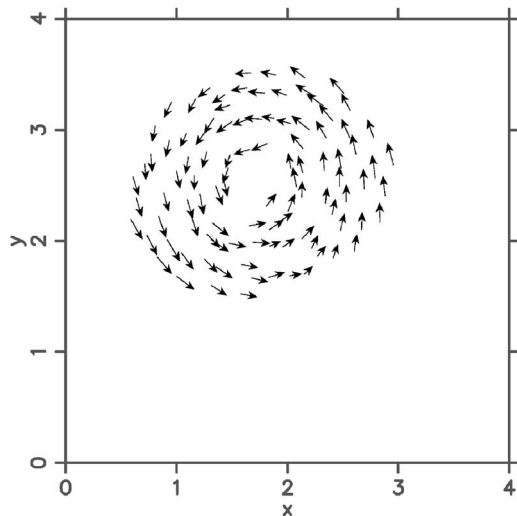
FIG. 4. A snapshot of a steady rotating flock. The particles are circulating around a common center in the same sense, with no directed motion as a whole. $N=100$, $L=10$, $a=1$, $r_a=0.001$, $b=1$, $w=2$.

vortex becomes unstable. The particles reassembled to make a marching flock.

Among these phases, the vortex in the absence of a confining boundary has been observed and analyzed in some detail in Ref. [11]. We note that all the flocking states other than the crystal phase have rather small basins of attraction in phase space. The associated phase boundaries are thus difficult to determine precisely. Besides, to obtain a phase diagram one has to address nasty issues such as finite-size effects and the interplay between the long-time and the thermodynamic limit. We shall postpone such considerations until a future work [18] in which we shall also discuss the appearance of patterned internal flow within a marching flock due to having variable-amplitude alignment as in (4). In the following, we shall focus on the vortex state alone, as it is probably the most interesting yet peculiar way to flock.

C. The vortex

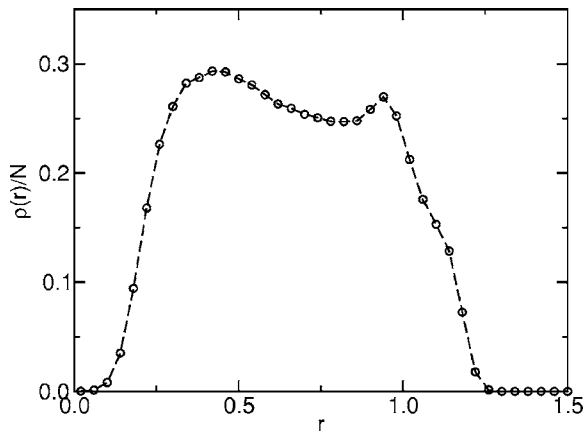To characterize the vortex state, one might address the questions of its stability and structure. At fixed parameter
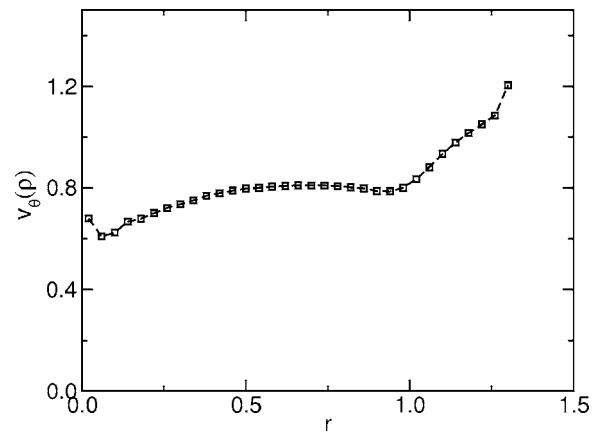

FIG. 6. Tangential velocity profile for a vortex. $N=100$, $L=10$, $a=1$, $r_a=0.001$, $b=1$, $w=2$.

values with random initial conditions, a certain fraction of samples will evolve into a vortex state, with the rest going into a drifting cluster (crystalline or swarmlike depending on the noise). That fraction may be taken as an indication of the relative size of the basin of attraction for the vortex and a drifting cluster. For some parameter values, we observe the vortex to form but decay into a drifting cluster within a finite time. At other values (e.g., at smaller r_a), the vortex may persist indefinitely. For all practical purposes, in certain regions of the parameter space, one may regard the vortex state as a stable steady state. For those stable vortices, we measure the profiles of the density $\rho(r)$, tangential velocity $v_\theta(r)$ and angular velocity $\omega(r)$ versus the radial distance r from the center of mass. Figures 5–7 display some typical results. To exhibit the balance of forces more clearly, we choose to eliminate the alignment effect by setting a vanishingly small alignment range (physically no difference from $r_a=0$) for those plots.

Density plots show that the flock has a well-defined hollow core and an outer layer, similar to what was found in [11]. Their sizes are largely determined by the speed a and the strength of the body force b. For smaller b, the size of the core increases because the resulting smaller body force is unable to sustain rotation at a small radius. Likewise, the

FIG. 5. Normalized density profile for a vortex. $N=100$, $L=10$, $a=1$, $r_a=0.0001$, $b=1$, $w=2$.
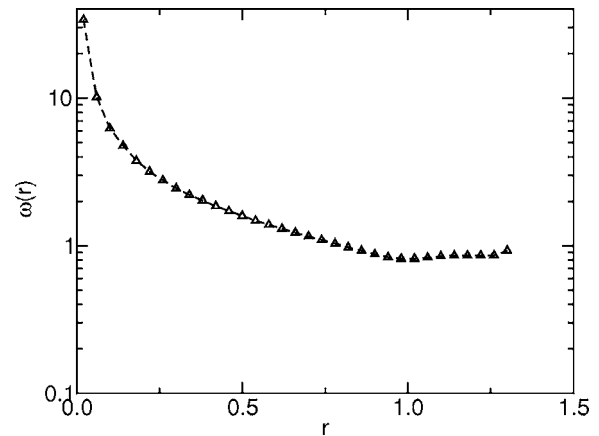

FIG. 7. Angular velocity profile for a vortex. $N=100$, $L=10$, $a=1$, $r_a=0.0001$, $b=1$, $w=2$.

core also increases with greater speed a. Near both edges there are small humps, also similar to [11]. As will be discussed in the next section in our phenomenological continuum theory, small humps in the particle density of rotating flocks is not universal, it depends on the details of the body force. In the bulk, the density is relatively uniform, at a value determined by balancing the body force with the centripetal force (see next section). Notice that $\rho \gg 1$ there because of the soft-core repulsion between the particles. The fact that the body force is attractive over some distance beyond $r=1$ (see Fig. 1) also contributes to high particle density in the flocks. Essentially, all the particles are interacting with each other. This situation is intensified for flocks with more particles—the particles are increasingly squeezed as the extent of the flock increases very slowly with respect to N.

The tangential velocity profile in the bulk is also nearly uniform. However, it deviates from the preferred speed due to nonzero radial component v_r, as an individual particle does not always stay at the same distance from the center, but rather dives in and out with respect to the flock spontaneously. This random motion contributes to the large v_θ near the core. Large v_θ at small r is impossible to sustain by the body force alone should $v_r = 0$. At the outer edge, there is a boundary layer where the velocity increases almost linearly. The reason for this increase is due to less repulsion (repulsive when the interparticle distance is smaller than unity), hence stronger centripetal force, experienced by a particle the farther away it is from the bulk. Except for the boundary layer, the angular velocity plot shows that the flock does not rotate as a solid body, for it would contradict with the fact that all particles try to move at the same speed fixed by the self-propulsion and the drag term in (1).

These results motivate us to study the continuum theory for a rotating flock. There are generally two routes to this end: One may coase-grain average the discrete model to obtain the continuum correspondence, in the form of a continuity equation for the density field and a Navier-Stokes-like equation for the velocity field, as done in [11]. In that approach, the interaction terms are expressed as spatial integrals over the distribution of particles. Alternatively, one may adopt a more phenomenological approach by writing down a continuum model based on symmetries and desired features for the interactions, in the spirit of Ginzburg-Landau, as pioneered by Toner and Tu [8]. Its advantage is that the resulting model, being completely local, is easier to analyze. In the next section, we shall consider such an approach.

III. CONTINUUM THEORY

Our continuum theory consider a group of N SPPs in a two-dimensional space with density $\rho(\mathbf{r}, t)$ and velocity field $\mathbf{v}(\mathbf{r})$. Therefore $\int d^2 r \rho(\mathbf{r}, t) = N$ and

$$\frac{\partial \rho}{\partial t} = -\boldsymbol{\nabla} \cdot \mathbf{J}, \qquad (5)$$

where $\mathbf{J} = \rho \mathbf{v}$, and $\mathbf{v}(\mathbf{r}, t)$ is the coarse-grained velocity field. The force acting on the particles in a flock is assumed to be the sum of three different types of forces. They are driving-

drag force $\mathbf{F}^{(d)}$, alignment force $\mathbf{F}^{(a)}$, and body force $\mathbf{F}^{(b)}$. Thus the equation for the velocity field takes the following form,

$$\frac{\partial \mathbf{v}}{\partial t} + \mathbf{v} \cdot \boldsymbol{\nabla} \mathbf{v} = \mathbf{F}^{(d)} + \mathbf{F}^{(a)} + \mathbf{F}^{(b)}. \qquad (6)$$

The driving-drag force $\mathbf{F}^{(d)}$ includes the self-propelling driving force and the drag force acting on these particles. The choice of $\mathbf{F}^{(d)}$ is not unique; in the present analysis we discuss two popular choices. A simple assumption is that the drag force is proportional to the local velocity field, and the driving force has a constant magnitude [15]; we call this choice "model I." Another choice is to emphasize the similarity between SPPs and XY-ferromagnets, thus a Ginzburg-Landau-like form for $\mathbf{F}^{(d)}$ is appropriate [8]. This choice is called "model II." Therefore

$$\mathbf{F}^{(d)} = v_0 \hat{\mathbf{v}} - \mathbf{v}, \quad \text{in model I,}$$

$$\mathbf{F}^{(d)} = (v_0^2 - v^2)\mathbf{v}, \quad \text{in model II.} \qquad (7)$$

In principle the existence of nonzero v_0 is a result of both self-propelling and velocity alignment, thus v_0 should be a function of ρ [8]. In the present model we focus on the case when magnitude of local velocity field is dominated by self-propelling and drag, and the alignment is included in the nonlocal terms in $\mathbf{F}^{(a)}$, thus v_0 is chosen to be a constant independent of ρ. This greatly simplifies our subsequent analysis. The alignment force written as an expansion in powers of $\mathbf{v}$ and ρ has the form

$$\mathbf{F}^{(a)} = \gamma_1 \rho \boldsymbol{\nabla}^2 \mathbf{v} + \gamma_2 \boldsymbol{\nabla} \rho \cdot \boldsymbol{\nabla} \mathbf{v} + \gamma_3 \boldsymbol{\nabla}^2 \rho \mathbf{v} + \cdots , \qquad (8)$$

where higher-order terms are neglected, and γ_i's are phenomenological parameters with dimension of length square. It is convenient to think of the γ_i's as the square of momentum density $(\rho \mathbf{v})$ correlation lengths. The body force has to be such that the system prefers to have a finite nonzero density in the absence of any other forces. An intuitive choice is

$$\mathbf{F}^{(b)} = c \boldsymbol{\nabla} (-\xi^2 \boldsymbol{\nabla}^2 \rho - \rho + \rho^2/\rho_0) \quad \text{(type-1 body force),} \qquad (9)$$

where ρ_0 is the preferred density of the flock in the absence of other forces, and ξ is a characteristic length which is analogous to the density correlation length in simple fluids. Close to the boundary of a flock the particle density ρ changes from ρ_0 to 0 within length scale ξ. It is clear that other choices of $\mathbf{F}^{(b)}$ are possible, thus Eq. (9) is called a "type-1 body force." We will show that the details of the density profile in a steady rotating flock do depend on the choice of $\mathbf{F}^{(b)}$. Another choice of body force (type-2 body force) that will be discussed in this paper is

$$\mathbf{F}^{(b)} = c \boldsymbol{\nabla} \left[-\xi^2 \boldsymbol{\nabla}^2 \rho - \left(\frac{\rho_0}{2}\right)^2 \left(\rho - \frac{\rho_0}{2}\right) \right.$$
$$\left. + \left(\rho - \frac{\rho_0}{2}\right)^3 \right] \quad \text{(type-2 body force).} \qquad (10)$$

Notice that in principle a term like $\kappa \boldsymbol{\nabla}^2 \mathbf{v}$, analogous to the usual viscosity, should be included on the right-hand side of

the momentum equation [1]. We assume that the contribution of velocity alignment is dominated by the interaction with the neighbors, therefore only terms that are linear in ρ are included in our theory. Similar approximation has been applied to other models for active biological systems [19].

To study 2D steady rotating flocks, we choose polar coordinates and look for steady-state solution of the form $\mathbf{v}(\mathbf{r}) = v(r)\hat{\theta}$ and $\rho(\mathbf{r}) = \rho(r)$. It happens that in the equations for steady rotating flocks, $\mathbf{F}^{(a)}$ does not have an r component and $\mathbf{F}^{(b)}$ does not have a θ component. Therefore the r component of the velocity equation becomes

$$\frac{v^2}{r} = F^{(b)}. \tag{11}$$

The physical meaning of this equation is clear: in the steady rotating state the body force is the centripetal force of the rotating flock. The θ component of the steady-state momentum equation is

$$0 = v_0 - v + F^{(a)}, \quad \text{model I,}$$

$$0 = (v_0^2 - v)v + F^{(a)}, \quad \text{model II.} \tag{12}$$

This equation tells us that the speed of the flock at r is determined by balancing the driving-drag term with alignment force. It is important to point out that although in the present analysis both type-1 and type-2 body forces are short-range forces, even when the body force is long range, $\mathbf{F}^{(b)}$ still has no tangential component due to the rotational symmetry of the system.

In general Eqs. (11) and (12), can be solved numerically only, and the solution depends on the parameters in the equations as well as the total number of particles in the system. However, in two special cases simple solutions with appealing physical features can be found. Therefore in the following we discuss these two special cases and postpone the analysis of general vortex solution to a future work [18].

A. Weak alignment limit

When γ_i's are small and negligible, the steady rotating flock solution becomes very simple because from Eq. (12), $v = v_0$ everywhere for both model I and model II flocks due to the absence of alignment force, and the radial component of the momentum equation becomes

$$\frac{v_0^2}{r} = F^{(b)}. \tag{13}$$

Notice that the centripetal acceleration diverges at $r = 0$ in this case. Therefore in the weak alignment limit the density of a steady rotating flock at its center has to vanish. $\rho(r)$ can be calculated by integrating Eq. (13) numerically under the constraint $\int d^2 r \rho(r) = N$. Figure 8 shows the numerical solutions of $\rho(r)$ for steady rotating flocks with type-1 body force, and $\rho_0 = 1$, $N \approx 2700$ in the weak alignment limit for $c = 0.01$ and $c = 0.1$, respectively. The size of the empty core decreases as the strength of the body force increases because stronger body force is able to provide the centripetal force for particles with smaller rotating radius. Figure 9 shows $\rho(r)$
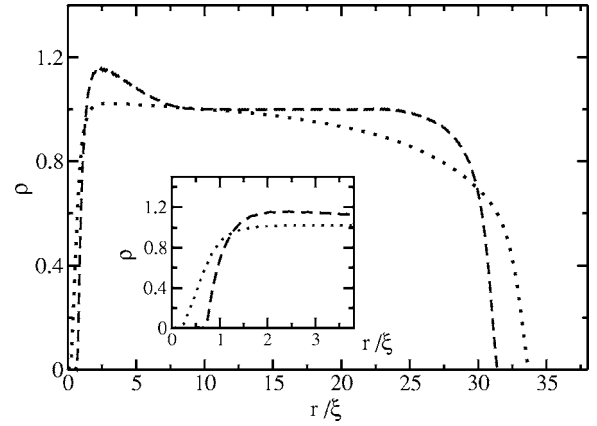

FIG. 8. Density profile $\rho(r)$ for steady rotating flocks in the weak alignment limit with $\rho_0 = 1$, $N \approx 2700$, and $c = 0.01$ for dashed curve, $c = 0.1$ for dotted curve. The inset shows density profiles for both flocks close to $r = 0$. The radius of empty core decreases as c increases because stronger body force can provide centripetal force for particles closer to the center of the flock.

for type-2 body force with $\rho_0 = 1$, $c = 0.01$, $N \approx 1100$, and $N \approx 2500$, respectively. The density profile for this choice of body force is different from Fig. 8; especially close to the outer boundary to the flock, ρ becomes greater than ρ_0. For sufficiently large flock the density of particles away from the inner and outer edges is close to ρ_0. Therefore it is clear that the details of the density profile in a steady rotating flock are not universal; they depend on the choice of body force, i.e., the details of the interparticle interactions. Density profiles similar to that of Fig. 9 have been seen in our particle-based simulation and Ref. [11]. However, there is an intrinsic difference between the discrete and the continuum models. The density in the bulk of a flock increases with the number of particles (N) in the discrete models, whereas by construction the interaction in the continuum model is short range, hence the density has a preferred value at large N. In view of this difference, at present we are not certain to what extent the similarity in the profiles between these models is generic for the rotating state.
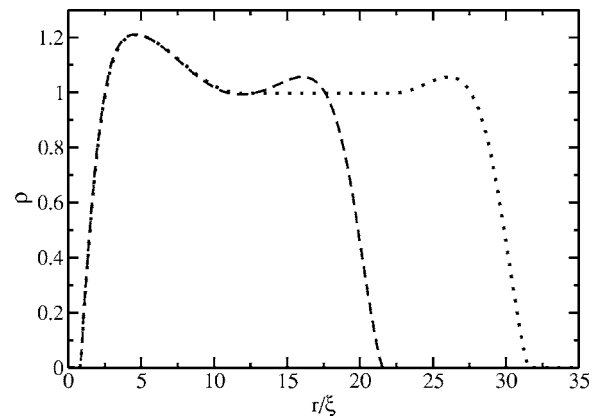

FIG. 9. Density profile $\rho(r)$ for a steady rotating flock in the weak alignment limit with $c = 0.01$, $\rho_0 = 1$, $N \approx 1100$ (dashed curve), and $N \approx 1500$ (dotted curve). The body force in this case is given by $\mathbf{F}^{(b)} = \nabla\left[-\xi^2\nabla^2\rho - \left(\frac{\rho_0}{2}\right)^2\left(\rho - \frac{\rho_0}{2}\right) + \left(\rho - \frac{\rho_0}{2}\right)^3\right]$.
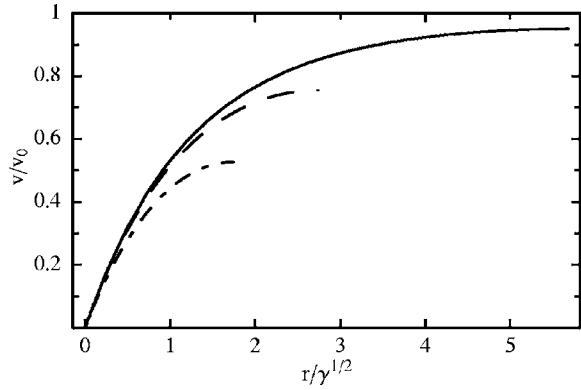
FIG. 10. Velocity profile $v(r)/v_0$ in Eq. (16) with $\alpha=0.45\frac{\pi}{2}$ (dash-dotted curve), $\alpha=0.49\frac{\pi}{2}$ (dashed curve), and $\alpha=0.499\frac{\pi}{2}$ (solid curve). The outer edge of the flocks are located at where $dv(r)/dr=0$.

B. Strong body force limit

As the density profiles of steady rotating flocks in the weak alignment limit show, the core radius of a flock becomes smaller as the strength of the body force increases because it becomes more and more difficult to make the density of the particles different from ρ_0. Therefore when the strength of body force, c, becomes very large but the γ_i's are not all negligible, the steady rotating flock solution becomes simple again. This is because from Eq. (11) it is clear that when c is very large, for any finite body force, $\rho(r)$ should be such that $F^{(b)}/c$ is vanishingly small everywhere. Therefore when flock size is large compared to ξ, we can approximate the density profile of a rotating flock by $\rho=\rho_0$ inside the flock, the radius of this flock is simply $r_0=(N/\pi\rho_0)^{1/2}$, and the velocity field is determined by

$$0 = v_0 - v + \gamma\left[\frac{1}{r}\frac{\partial}{\partial r}\left(r\frac{\partial}{\partial r}\right)v - \frac{v}{r^2}\right] \quad \text{for model I,} \quad (14)$$

and

$$0 = (v_0^2 - v^2)v + \gamma\left[\frac{1}{r}\frac{\partial}{\partial r}\left(r\frac{\partial}{\partial r}\right)v - \frac{v}{r^2}\right] \quad \text{for model II.}$$

$$(15)$$

Here $\gamma=\gamma_1+\gamma_3$ and the velocity field satisfies free boundary condition $\partial v/\partial r=0$. The solution of Eq. (14) is a linear combination of $I_1(r/\gamma^{1/2})$, the modified Bessel function of order one, and $L_1(r/\gamma^{1/2})$, the modified Struve function of order one,

$$v(r/\gamma^{1/2}) = \alpha I_1(r/\gamma^{1/2}) - \frac{\pi}{2}L_1(r/\gamma^{1/2}), \quad (16)$$

where the constant α should be chosen such that $dv/dr=0$ at $r=r_0$. Figure 10 shows Eq. (16) for different choices of α. As r_0 increases, α approaches $\pi/2$ from below, and the maximum speed in the flock approaches v_0 as r_0 increases. This velocity profile is similar to that obtained in Ref. [15], although the model in Ref. [15] describes the dynamics of bacteria colonies on a substrate, and the height of the colony is allowed to be different at different points, while our model

studies a true two-dimensional SPP system: there is no variable associated with the thickness of the system.

Let us now turn our attention to model II. Mathematically Eq. (15) is equivalent to minimizing a Ginzburg-Landau free-energy-like functional

$$G[v] = \int_0^{r_0} d^2r\left(\frac{\gamma}{2}(\nabla v)^2 - \frac{1}{2}v_0^2v^2 + \frac{v^4}{4}\right). \quad (17)$$

Since $G=0$ for a stationary flock ($v=0$ everywhere), the rotating flock solution for model II exists only when the solution of Eq. (15) satisfies $G[v]<0$. The local part of $G[v]$ is negative for $0<v<v_0$, thus the rotating flock solution should exist for sufficiently large flocks because the nonlocal part of $G[v]$, which is positive, comes mostly from the small r region of the flock. Figure 11 shows the numerical solution of $v(r)$ for model II with $r_0=10\gamma^{1/2}$ and $r_0=4\gamma^{1/2}$ (inset). The maximum speed in the flock increases as the size of the flock increases. For large flocks the maximum speed in the flock is close to v_0.

It is interesting to discuss the huge difference of the maximum speed in small rotating flocks between Figs. 11 and 10. The maximum speed of a small rotating model I flock is much greater than the maximum speed of a small rotating model II flock. This difference comes from the local part of the equation for $v(r)$. For a rotating model II flock, $v(r)$ comes from balancing the Laplacian of v with $v_0^2v-v^3$. Since at small r, $v \ll v_0$, therefore the Laplacian at small r is on the order of $v_0^2v \sim v$, which is also small. Thus $v(r)$ increases slowly at small r, and the maximum speed inside a small model II flock is much smaller than v_0. On the other hand, $v(r)$ for a rotating model I flock comes from balancing the Laplacian of v with v_0-v. At small r, $v_0-v \sim v_0 \gg v$, thus the Laplacian of v is not small at small r. Thus $v(r)$ increases faster for rotating model I flocks than rotating model II flocks, and the maximum speed of a small rotating model I flock is much greater than that of a small rotating model II flock.
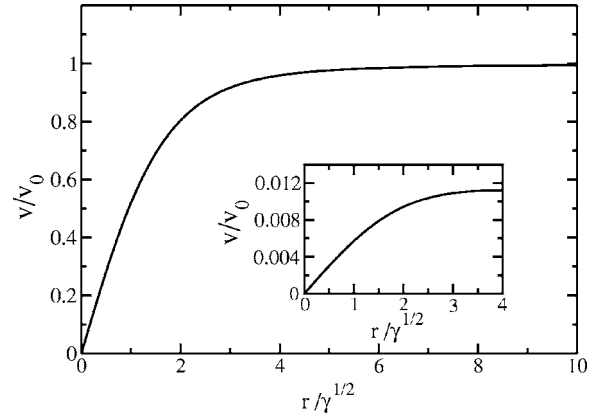

FIG. 11. Velocity profile $v(r)/v_0$ for a steady rotating flock in the strong body force limit of model II with $r_0=10\gamma^{1/2}$. The inset shows the velocity profile for a flock with $r_0=4\gamma^{1/2}$. The maximum speed in the small flock is much smaller than the maximum speed in the large flock.

Mikhailov and Calenbuhr constructed a similar hydrodynamic model (MC model) for two-dimensional self-propelling particles in Ref. [1] and have predicted some properties of the velocity and density profiles of the rotating states. In the MC model, the momentum equation has Ginzburg-Landau-type driving-drag terms. However, the alignment force between the particles is not included in the model; instead, the density-independent viscous term is kept in the momentum equation. The boundary condition for a finite-size flock with no bounding walls is chosen such that the normal stress at the edge of the flock satisfies the Gibbs-Thompson relation (which is true when the density profile is not very far from a condensed flock with no driving and drag). Since the alignment force is not included in the MC model, the predictions in Ref. [1] are supposed to apply to situations different from our current study. However, the MC model shows that in the presence of viscosity, the magnitude of the velocity field for rotating states rises from zero at $r=0$ and saturates when r is large compared to the velocity correlation length defined by the viscosity term. The density profile also rises from a small value at $r=0$. These features are common to both the MC model and our model.

IV. SUMMARY

We have studied the flocking behavior of SPPs in two-dimensional space by particle-based simulations and a phenomenological continuum theory with special attention devoted to the rotating states. In the particle-based simulations, we find that marching flocks are ubiquitous and rotating flocks are observed only when both the range and strength of the alignment interaction are small. Thus our study reveals the reason why the models of Toner, Tu, and collaborators [8–10] did not yield finite-size rotating flocks in free space but Levine *et al.* [11] reported observing vortices in a range of parameters: In Ref. [11] the vortices are observed when the alignment interaction is very weak; on the other hand, the authors of Refs. [8–10] consider the case when alignment is the key interaction for flocking, thus no rotating flocks are observed. We find that the density profile for rotating flocks with vanishingly weak alignment, short-range, soft-core repulsion, and long but finite range attraction in our simulations is similar to Ref. [11], where the short-range repulsion between the particles is also of finite strength. The tangential velocity field of rotating flocks is fairly uniform except close to the inner and outer edges of the flock. The angular velocity profile reveals that the flock does not rotate like a rigid body due to the liquid-like spatial correlation.

In the continuum theory, the radial component of the velocity equation is simply the balance between the body force and the centripetal acceleration, and the tangential component of the velocity equation reveals that the velocity profile is determined by balancing the driving-drag force with the alignment force. The rotating state solutions become simple in the weak alignment or strong body force limits. In the weak alignment limit, particle density vanishes near the center of the flock due to the divergence of the centripetal force. In general the density profile depends on details of the body force. For different choices of body force, rotating flocks with density profiles that contain a hump near the central core or two humps, one near the center another near the edge, are observed. Comparing to Ref. [11], our study points out that the existence of an empty core in the weak limit is universal, but the characteristics of the density of profile is model dependent. A prediction for the size of the empty core is not available in the present analysis and it will be postponed until a future work. In the strong body force limit, the system is incompressible and the density is uniform across the flock. The velocity field rises from zero at the center to its maximum value at the edge of the flock. The maximum velocity in a flock increases with the size of the flock. The maximum velocity of small flocks (where flock radius is on the same order as the velocity correlation length) also depends strongly on the details of the driving-drag force in the small v limit.

There are a couple of interesting questions to be answered in the future. For example, it is clear that the parameter range under which stable rotating flocks form is quite limited; especially, it also depends on the number of particles in the system. It has been reported that for systems with a large number of particles, several rotating flocks instead of a big one form [15]. Therefore the stability of rotating flocks is still an interesting open question. With current studies mostly devoted to two-dimensional SPP flocks, the robustness of a rotating flock against the freedom of a third dimension is also an important but unanswered question. We expect the lack of translational invariance in the third dimension introduces new effects that are not present in two-dimensional models. Finally, the response of flocks to disturbance such as external flow field is of great interest, too. These questions point out the direction of our future work.

[1] A. S. Mikhailov and V. Calenbuhr, *From Cells to Societies* (Springer-Verlag, Berlin, 2002).

[2] M. Matsushita, J.-I. Wakita, and T. Matsuyama, in *Spatio-Temporal Patterns in Nonequilibrium Complex Systems*, edited by P. E. Cladis and P. Palffy-Muhoray, Santa Fe Institute Studies in the Sciences of Complexity (Addison-Weseley, Reading, MA, 1995), pp. 609–618.

[3] E. Ben-Jacob, I. Cohen, and H. Levine, Adv. Phys. **49**, 395 (2000).

[4] J. K. Parrish, S. V. Viscido, and D. Grünbaum, Biol. Bull. **202**,

296 (2002).

[5] J. Toner, Y. Tu, and S. Ramaswamy, Ann. Phys. **318** (1), 170 (2005).

[6] W.-J. Rappel, A. Nicol, A. Sarkissian, H. Levine, and W. F. Loomis, Phys. Rev. Lett. **83**, 1247 (1999).

[7] N. Shimoyama, K. Sugawara, T. Mizuguchi, Y. Hayakawa, and M. Sano, Phys. Rev. Lett. **76**, 3870 (1996).

[8] J. Toner and Y. Tu, Phys. Rev. Lett. **75**, 4326 (1995).

[9] J. Toner and Y. Tu, Phys. Rev. E **58**, 4828 (1998).

[10] G. Grégoire, H. Chaté, and Y. Tu, Physica D **181**, 157 (2003).

[11] H. Levine, W.-J. Rappel, and I. Cohen, Phys. Rev. E **63**, 017101 (2000).

[12] U. Erdmann, W. Ebeling, and V. S. Anishchenko, Phys. Rev. E **65**, 061106 (2002).

[13] R. Mach, A. Ordemann, and F. Schweitzer, e-print q-bio.PE/0404028.

[14] A. Ordemann, G. Balazsi, and F. Moss, Nova Acta Leopold. **88**, 332 (2003).

[15] Z. Csahók, and A. Czirók, Physica A **243**, 304 (1997).

[16] W.-T. Juan, Z.-H. Huang, J.-W. Hsu, Y.-J. Lai, and L. I., Phys. Rev. E **58**, R6947 (1998).

[17] See, e. g., http://www.oceanlight.com/html/schooling.html.

[18] K.-t. Leung and H. Y. Chen (unpublished.)

[19] H. Y. Lee and M. Kardar, Phys. Rev. E **64**, 056113 (2001).